

Parametric Frequency Conversion in Layered Nonlinear Media

G. Kh. Kitaeva and A. N. Penin

Moscow State University, Moscow, 119992 Russia

e-mail: kit@gopt.phys.msu.su

Received May 22, 2003

Abstract—Frequency-angular distributions of signal wave intensity are calculated for spontaneous parametric down-conversion and parametric frequency conversion in spatially nonuniform nonlinear media. Wave reflection from interfaces is taken into account, and both regular and irregular nonuniform distributions of second-order nonlinear susceptibility are considered. A unified approach using a scattering matrix and a generalized Kirchhoff law is applied in calculations of spontaneous and stimulated processes in dissipative nonlinear media. Interference of electromagnetic zero-point fluctuations of the vacuum, nonlinear interference and nonlinear diffraction are examined for media with various absorptive properties. Theoretical foundations are developed for diagnostics of nonuniform distributions of the second-order susceptibility, based on measurement of the line profiles of nonlinear signals. © 2004 MAIK “Nauka/Interperiodica”.

1. INTRODUCTION

Media with spatially varying linear and nonlinear optical properties are currently attracting great attention [1, 2]. They are widely used in nonlinear optics and laser physics [3–9]. Characteristics of parametric processes in crystals with deep modulation of the second-order nonlinear susceptibility are the subject of ongoing research [3, 4, 6–8]. In our view, progress in this area is important for laser spectroscopy of solids and polymers, because parametric processes offer novel opportunities for analyzing the structure of inhomogeneous multidomain crystals and polymer materials and their transformations [9].

Spatial nonuniformity (periodic or random, depending on a particular specimen) strongly affects the nonlinear optical processes in which phase matching is a necessary condition. Energy conservation is a strict requirement. Under steady-state conditions, it reduces to zero sum of the frequencies of the interacting waves. By contrast, momentum conservation may hold up to a certain mismatch when part of the momentum carried by light waves is transferred to the medium. In the general case, parametric processes in inhomogeneous media depend on changes in linear and nonlinear optical parameters across interfaces, geometry of individual regions, characteristics of boundaries, scattering and absorption coefficients, the coefficients characterizing nonlinear optical conversion, etc. Analysis of the integral effect of the combination of all factors on two- or three-dimensional scattering spectrum is a difficult task. The problem is substantially simplified by invoking the generalized Kirchhoff law (a nonlinear analogue of the Kirchhoff law) formulated by Klyshko [10, 11] in the framework of a unified phenomenological approach to

spontaneous and stimulated parametric interactions in weakly nonlinear dissipative media. The generalized Kirchhoff law can be used to determine second-order correlation functions for the output field by using the corresponding functions prescribed at the input end and to calculate both frequency-angular distribution of the output radiation intensity and its statistical characteristics. In calculations of this kind, a linear relationship between the Heisenberg operators of the input and output fields is postulated. (The only exception is the pump field, which is treated as a classical wave of prescribed intensity.) This relationship is formulated in terms of a scattering matrix. The matrix can be calculated within the framework of classical nonlinear optics, and its elements determine the relations between the classical field strengths for all input and output modes.

In this paper, we present the results obtained by applying the generalized Kirchhoff law to parametric processes in media with nonuniform distributions of optical parameters. We consider spontaneous parametric down-conversion (SPDC) and parametric frequency conversion (PC) in media without inversion center [10]. SPDC is the scattering or decay of pump photons of frequency ω_0 caused by quantum field fluctuations in a medium with nonzero second-order nonlinear susceptibility $\chi^{(2)}$.¹ As a result, photon pairs correlated with respect to the time and location of their origin are created in the medium. The frequencies of these photons, ω_1 and ω_2 , are related as follows:

$$\hbar\omega_0 = \hbar\omega_1 + \hbar\omega_2. \quad (1)$$

¹ SPDC was predicted by Klyshko in a paper presented in 1966 at the All-Union Conference on Nonlinear Media in Chernogolovka.

Their propagation directions are determined by the phase matching condition

$$\mathbf{k}_0 = \mathbf{k}_1 + \mathbf{k}_2 - \Delta\mathbf{k}, \quad (2)$$

where $\mathbf{k}_j \equiv n_j\omega_j/c$ is the j th wave vector and n_j is the refractive index at ω_j ($j = 0, 1, 2$). The frequencies ω_1 and ω_2 may vary from zero to ω_0 . By convention, the wave with frequency between $\omega_0/2$ and ω_0 is called signal wave (ω_1) and the other one, with frequency below $\omega_0/2$, is called idler wave (ω_2). Normally, the frequency of the signal wave generated in an experiment lies in a range well suited for measurement. The phase matching condition for the wave vectors \mathbf{k}_j is satisfied up to a mismatch $\Delta\mathbf{k}$ that depends on absorption, geometry of the illuminated specimen, and dispersion of refractive index.

The emergence of photons at ω_1 and ω_2 via SPDC (without any input at these frequencies) can be explained only in the framework of a consistent quantum-theoretic treatment. Outside the absorption band, scattered radiation leaves the medium, consisting of correlated photon pairs (biphotons) [15, 16]. SPDC can be interpreted as the result of scattering of the pump wave by electromagnetic fluctuations of the vacuum in a nonlinear medium. If one of the output frequencies lies in an absorption band, e.g., a photon resonance absorption band, then a photon–polariton pair is created. In this case, the pump is scattered both by vacuum fluctuations and by thermal fluctuations of the scattering medium [17, 18]. When the input contains not only pump, but also a signal- or idler-frequency wave, then spontaneous light scattering is accompanied by parametric decay of pump photons into biphotons. In contrast to SPDC, parametric frequency conversion can be described by both quantum and classical models [19].

Here, we use the generalized Kirchhoff law in analyzing some specific effects of spatial inhomogeneity on SPDC and PC spectra. In Section 2, we apply the generalized Kirchhoff law to calculate the signal line profile in the simplest case of a slab of nonlinear medium. This model was examined previously in analyses based on different approaches [10]. The present study includes calculation of the scattering matrix and provides a methodological basis for further analysis. In Section 3, we calculate the frequency-angular distributions for SPDC and PC signal waves in a slab with reflecting boundaries [20]. We analyze the fine interference structure of line profiles for various cases of signal and idler absorption. Next, we consider the effects of electromagnetic zero-point fluctuations of the vacuum (Section 4) and spatial distribution of the effective second-order susceptibility (Section 5) on the SPDC spectrum.

The present study is focused on the characteristics of three-wave SPDC and parametric difference-frequency generation in a spatially nonuniform medium. However, the results obtained for difference-frequency

generation can be modified to describe optical harmonic generation and sum-frequency generation, as well as cascade processes of higher orders, in the constant-pump approximation by assuming linear amplification of the remaining waves.

2. SCATTERING MATRIX AND SIGNAL LINE PROFILE IN A SLAB

For three-wave parametric interactions, the average number of signal and idler output photons, $N_{1'} \equiv \langle a_{1'}^\dagger a_{1'} \rangle$ and $N_{2'} \equiv \langle a_{2'}^\dagger a_{2'} \rangle$, dictated by the generalized Kirchhoff law is

$$N_{1'} = \hat{U}_{1'1}(N_1 + N_0 + I)\hat{U}_{1'1}^\dagger - \hat{U}_{1'2}(\tilde{N}_2 - N_0)\hat{U}_{1'2}^\dagger - N_0 - I, \quad (3)$$

$$N_{2'} = \hat{U}_{2'1}(\tilde{N}_1 + N_0 + I)\hat{U}_{2'1}^\dagger - \hat{U}_{2'2}(N_2 - N_0)\hat{U}_{2'2}^\dagger + N_0, \quad (4)$$

where I is the identity matrix and \hat{U}_{ij} is an entry of the scattering matrix

$$\hat{U} = \begin{pmatrix} \hat{U}_{1'1} & \hat{U}_{1'2} \\ \hat{U}_{2'1} & \hat{U}_{2'2} \end{pmatrix}.$$

The subscripts 1' and 2' run through all signal and idler output modes; the subscripts 1 and 2, through all corresponding input modes;

$$(N_1)_{ij} \equiv \langle a_{1i}^\dagger a_{1j} \rangle, \quad (N_2)_{ij} \equiv \langle a_{2i}^\dagger a_{2j} \rangle$$

are the matrices representing the second-order moments of the input field; \tilde{N}_1 and \tilde{N}_2 are transposed matrices; a_k^\dagger and a_k are the creation and annihilation operators for k th-mode photons;

$$N_0 \equiv 1/[\exp(\hbar\omega_p/kT) - 1]$$

is the temperature factor, where ω_p is the phonon resonance frequency. Normally, this factor can be neglected since it is much less than unity at room temperature. The difference between expressions (3) and (4) is due to the assumption that only idler waves are absorbed. This assumption is more likely to hold for real processes, as compared to substantial signal or pump absorption.

The scattering matrix \hat{U} defines a relationship between the creation and annihilation operators for the

input and output fields and their first-order moments, $(\langle a_1^\dagger \rangle, \langle a_2 \rangle)$ and $(\langle a_1^\dagger \rangle, \langle a_2 \rangle)$:

$$\begin{aligned} \langle a_1^\dagger \rangle &= \hat{U}_{11} \langle a_1^\dagger \rangle + \hat{U}_{12} \langle a_2 \rangle, \\ \langle a_2 \rangle &= \hat{U}_{21} \langle a_1^\dagger \rangle + \hat{U}_{22} \langle a_2 \rangle. \end{aligned} \quad (5)$$

Each mode satisfies the following relations outside the nonlinear medium up to general normalization factors:

$$\langle a_j^\dagger \rangle \sim \langle a_j \rangle \sim A_j \equiv E_j \sqrt{\frac{\cos \theta_j}{\omega_j}},$$

where θ_j is the angle of wave incidence (the angle between the normal vector to the surface and the pump wave vector). In the absence of scattering, the scattering matrix is unitary and

$$\hat{U} \hat{\sigma} \hat{U}^\dagger = \hat{\sigma},$$

where $\sigma_{mn} = (-1)^{m+1} \delta_{mn}$ (δ_{mn} is Kronecker's delta). Each element of the matrix can be determined experimentally. However, it is frequently sufficient to calculate these elements theoretically by solving equations for slowly varying field amplitudes. Substituting the resulting elements of \hat{U} into (3) and finding the average number of photon for each output mode, one can calculate the output signal intensity $P_{\omega\Omega}$ as a function of frequency and scattering (observation) angle, i.e., the line profile or form factor. (Intensity is defined as the energy emitted by a unit surface area into unit solid angle per unit spectral interval per unit time.) The output signal intensity is

$$P_{\omega_1\Omega_1} = \frac{\hbar \omega_1^3 \cos \theta_1}{c^2 \nu} N_{1'}, \quad (6)$$

where ν is the average volume per mode in the wave-vector space. Accordingly, the signal received with a quantum detector efficiency η_1 in the far-field region is

$$P_1 = \int_{\Delta\omega_{\text{det}}} d\omega_1 \int_{\Delta\Omega_{\text{det}}} d\Omega_1 \xi_1(\omega_1, \Omega_1) P_{\omega_1\Omega_1}, \quad (7)$$

where $\xi_1(\omega_1, \Omega_1) \equiv \eta_1 / \hbar \omega_1 c \cos \theta_1$. The integral is calculated over the bandwidth and aperture of the detector, $(\Delta\omega_{\text{det}})$ and $(\Delta\Omega_{\text{det}})$.

The correlation moment $K' \equiv \langle a_1 a_2 \rangle^*$, which determines the statistical properties of the output biphoton field, is expressed as

$$\tilde{K} = \hat{U}_{21} (\tilde{N}_1 + N_0 + I) \hat{U}_{11} + \hat{U}_{22} (N_2 - N_0) \hat{U}_{12}. \quad (8)$$

The moments $N_{1'}$ and $N_{2'}$ and the second-order correlator K' determine the fourth-order moment of the scattered field,

$$\langle a_{1_i}^\dagger a_{1_i} a_{2_m}^\dagger a_{2_m} \rangle = N_{1_i 1_j'} N_{2_m 2_n'} + K_{1_i 2_m'} K_{1_j 2_n'}^*,$$

which characterizes the correlation between signal and idler photons. It can be found by measuring the cross correlation of the signal and idler detector outputs [15, 16].

Consider a strong pump wave $E_0 \exp(i\mathbf{k}_0 \cdot \mathbf{r} - i\omega_0 t)$ and much weaker signal and idler waves $E_{10} \exp(i\mathbf{k}_1 \cdot \mathbf{r} - i\omega_1 t)$ and $E_{20} \exp(i\mathbf{k}_2 \cdot \mathbf{r} - i\omega_2 t)$ incident on a slab of thickness l . In the constant-pump approximation, the reduced wave equations describing the process are written as follows [21]:

$$\begin{aligned} \frac{dE_1(z)}{dz} + i\sigma_1 E_0 E_2^*(z) \exp\left(-\frac{iz\Delta}{l}\right) + \frac{y_1}{l} E_1(z) &= 0, \\ \frac{dE_2(z)}{dz} + i\sigma_2 E_0 E_1^*(z) \exp\left(-\frac{iz\Delta}{l}\right) + \frac{y_2}{l} E_2(z) &= 0. \end{aligned} \quad (9)$$

Here,

$$\Delta \equiv l(|k_{1z}| + |k_{2z}| - |k_{0z}|) \equiv \delta_1 + \delta_2 - \delta_0$$

is the dimensionless wave-vector mismatch, $\sigma_j \equiv 2\pi\chi\omega_j/cn_j \cos \vartheta_j$, and $y_j \equiv \alpha_j l / 2 \cos \vartheta_j$. The convolution of second-order nonlinear susceptibility tensor $\hat{\chi}^{(2)}$ with signal, idler, or pump unit polarization vectors is denoted by χ ; α_j denotes the absorption coefficient at the frequency ω_j ; and ϑ_j is the angle between the normal vector to the surface and a particular wave vector inside the slab. In the case of weak absorption, α_j is related to the imaginary part of permittivity ϵ_j'' as follows: $\alpha_j = \omega_j \epsilon_j'' / cn_j$.

Interaction between $E_1(z)$, $E_2(z)$, and $E_0 \exp(i\mathbf{k}_0 \cdot \mathbf{r} - i\omega_0 t)$ can be described by the parametric interaction matrix \hat{w} relating plane waves satisfying conditions (1) and (2):

$$\begin{pmatrix} A_1(l/2) \\ A_2(l/2) \end{pmatrix} = \begin{pmatrix} w_{11} & w_{12} \\ w_{21} & w_{22} \end{pmatrix} \begin{pmatrix} A_1(-l/2) \\ A_2(-l/2) \end{pmatrix}. \quad (10)$$

where

$$A_{1,2}\left(\pm\frac{l}{2}\right) \equiv E_{1,2}\left(\pm\frac{l}{2}\right) \sqrt{\frac{\cos \theta_{1,2}}{\omega_{1,2}}},$$

with $E_{1,2}(-l/2)$ and $E_{1,2}(l/2)$ denoting input and output wave amplitudes. Since the matrix \hat{w} is identical to \hat{U} in the case under analysis, its elements are expressed as follows by virtue of (9):

$$\begin{aligned} w_{11} &= e^{-\mu} \left(\cosh \gamma + \frac{\eta \sinh \gamma}{\gamma} \right)_1, \\ w_{22} &= e^{-\mu^*} \left(\cosh \gamma - \frac{\mu \sinh \gamma}{\gamma} \right), \end{aligned} \quad (11)$$

$$w_{12} = -i\beta e^{-\gamma/2} \frac{\sinh \gamma}{\gamma}, \quad w_{21} = i\beta^* e^{-\gamma/2} \frac{\sinh \gamma}{\gamma},$$

where

$$\begin{aligned} y &\equiv y_1 + y_2, \quad \mu \equiv (y_1 + y_2 + i\Delta)/2, \\ \eta &\equiv (-y_1 + y_2 + i\Delta)/2, \\ \gamma &\equiv \sqrt{|\beta|^2 + |\eta|^2}, \\ \beta &\equiv \frac{2\pi\omega_1\omega_2\chi l E_0}{c^2 \sqrt{k_{1z}k_{2z}}} \frac{\sqrt{\cos\theta_0}}{\sqrt{n_0 \cos\vartheta_0}}. \end{aligned} \quad (12)$$

In cases of experimental interest, only the lowest order terms can be retained in the power series expansions of \hat{w} . Then,

$$\begin{aligned} w_{11} &\approx e^{-y_1} + |\beta|^2 f_1(\eta), \\ w_{22} &\approx e^{-y_2} + |\beta|^2 f_2(\eta), \\ w_{12} &\approx i\beta f(\eta), \quad w_{21} \approx -i\beta^* f(\eta), \end{aligned} \quad (13)$$

where

$$\begin{aligned} f_1(\eta) &\equiv \frac{1}{(2\eta)^2} [e^{-y_2 - i\Delta} - (1 - 2\eta)e^{-y_1}], \\ f_2(\eta) &\equiv \frac{1}{(2\eta)^2} [e^{-y_1 + i\Delta} - (1 + 2\eta)e^{-y_2}], \\ f(\eta) &\equiv \frac{1}{2\eta} [e^{-y_2 - i\Delta/2} - e^{-y_1 + i\Delta/2}]. \end{aligned} \quad (14)$$

When only idler waves are absorbed, the generalized Kirchhoff law entails the following energy relation between SPDC signal characteristics:

$$N_{\Gamma}^{\text{SPDC}} = |w_{11}|^2 - 1.$$

By virtue of (6) and (13), this leads to the following expression for SPDC intensity in the linear approximation with respect to pump:

$$P_{\omega_1\Omega_1}^{\text{SPDC}} \Big|_{\substack{y_1=0 \\ y_2 \neq 0}} = C_{0g}(\Delta, y_2), \quad (15)$$

where

$$\begin{aligned} g(\Delta, y_2) &\equiv \frac{2}{(\Delta^2 + y_2^2)^2} [(\Delta^2 - y_2^2)(1 - e^{-y_2} \cos\Delta) \\ &\quad - 2y_2\Delta e^{-y_2} \sin\Delta + y_2(\Delta^2 + y_2^2)] \end{aligned} \quad (15')$$

is the form factor that determines signal intensity as a function of phase mismatch. The coefficient C_0 depends on pump intensity P_0 , specular transmissivity t_0^2 of the input surface, the layer thickness, and the effective second-order susceptibility χ :

$$C_0 \equiv \frac{\hbar\omega_1^4\omega_2}{c^5 n_0 n_1 n_2} P_0 t_0^2 \chi^2 l^2 \frac{\cos\theta_0 \cos\theta_1}{\cos\vartheta_0 \cos\vartheta_1 \cos\vartheta_2}.$$

For parametric conversion of an idler input of radiance N_2 , we have $N_{\Gamma} + N_{\Gamma}^{\text{SPDC}} + N_{\Gamma}^{\text{PC}}$, where N^{SPDC} is spontaneous ‘‘noise’’ and $N_{\Gamma}^{\text{PC}} = |\omega_{12}|^2 N_2$ is the PC signal radiance measured in units of number of photons per mode. In the linear (spontaneous–stimulated) regime of conversion, the corresponding intensity is

$$P_{\omega_1\Omega_1}^{\text{PC}} \Big|_{\substack{y_1 \neq 0 \\ y_2 \neq 0}} = C_0 F(\Delta, y_1, y_2) N_2, \quad (16)$$

where

$$\begin{aligned} &F(\Delta, y_1, y_2) \\ &\equiv \frac{\exp(-2y_1) - 2\exp[-(y_1 + y_2)] \cos\Delta + \exp(-2y_2)}{(y_1 - y_2)^2 + \Delta^2} \end{aligned}$$

is the form factor describing the observed spectrum corrected for absorption at both signal and idler frequencies. In particular, if only idler waves are absorbed, then the line profile due to parametric conversion characterized by an isotropic input intensity distribution (when all modes in the idler channel are uniformly populated) is

$$\begin{aligned} &F(\Delta, 0, y_2) \\ &\equiv \frac{1 - 2\exp(-y_2) \cos\Delta + \exp(-2y_2)}{y_2^2 + \Delta^2}. \end{aligned} \quad (16')$$

Expressions (15') and (16') for the SPDC and PC form factors imply that the line profiles of isotropic SPDC and PC waves are different in the case of non-zero, but weak, absorption at the idler frequency ($y_2 \sim 1$). It should be noted here that absorption at a signal frequency does not entail any distinction of this kind. However, the SPDC and PC line profiles are similar in the case of strong absorption at the idler frequency ($y_2 \gg 1$). Then, both waves have Lorentzian profiles as functions of the wave-vector mismatch:

$$\begin{aligned} P_{\omega_1\Omega_1}^{\text{SPDC}} \Big|_{\substack{y_1=0 \\ y_2 \gg 1}} &= C_0 N_2 \left(\frac{1}{y_2^2 + \Delta^2} \right), \\ P_{\omega_1\Omega_1}^{\text{PC}} \Big|_{\substack{y_1=0 \\ y_2 \gg 1}} &= C_0 N_2 \left(\frac{1}{y_2^2 + \Delta^2} \right). \end{aligned} \quad (17)$$

When the medium is transparent at all frequencies, we obtain well-known expressions for spontaneous [10] and

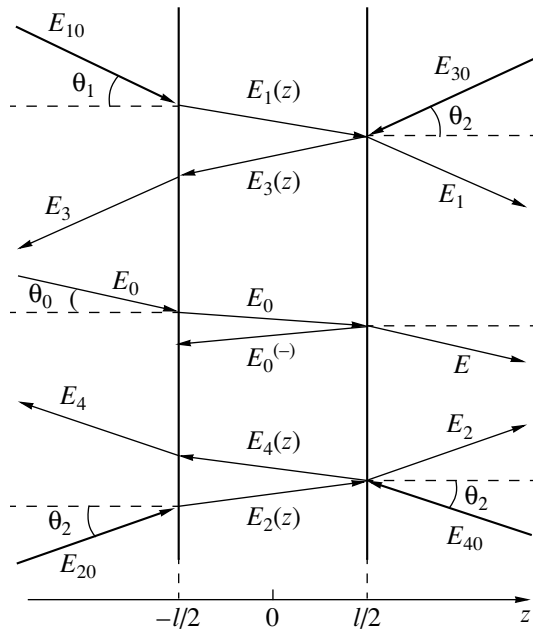


Fig. 1. Diagrams of waves propagating outside and inside a reflecting slab.

stimulated [19] waves as functions of the mismatch:

$$P_{\omega_1\Omega_1}^{\text{SPDC}} \Big|_{\substack{y_1=0 \\ y_2=0}} = C_0 \text{sinc}^2 \frac{\Delta}{2},$$

$$P_{\omega_1\Omega_1}^{\text{PC}} \Big|_{\substack{y_1=0 \\ y_2=0}} = C_0 N_2 \text{sinc}^2 \frac{\Delta}{2},$$
(18)

where $\sin x = \text{sinc} x/x$.

When the slab is transparent, the angular frequency bandwidths of these waves depend only on its thickness. In the case of substantial absorption (condition $y_j \ll 1$ is violated for $j = 1$ and/or $j = 2$), the widths are determined by both thickness and absorption coefficients α_j for the slab material. As an example, consider the line shape characteristics for signal with a wavelength of 625 nm when parametric interaction of *ooe* type takes place inside a slab of KDP crystal parallel to the z axis. The pump has extraordinary polarization and a wavelength of 488 nm and propagates along the normal to the slab. KDP crystal is virtually transparent for pump and signal in the visible range. The corresponding idler wavelength is 2.23 μm . The idler absorption coefficient is $\alpha_2 \approx 0.5 \text{ cm}^{-1}$. Expressions (18) apply to slabs of thickness between 0.1 and 2 cm (the line profile scales with $\text{sinc}^2(\Delta/2)$). The spectral width for the principal maximum in the signal profile emitted by a 1 cm thick slab is 0.5 nm, and the corresponding angular width is 0.03° . When the slab thickness is ten times smaller (1 mm), these widths are 5.4 nm and 0.35° , respectively. With decreasing signal wavelength, the idler wavelength increases and the absorption coefficient

α_2 grows even faster. For example, if signal is detected at 572 nm, then the idler wavelength is 3.32 μm . When $\alpha_2 \approx 100$ expressions (17) apply to slabs of thickness 0.5 and larger. The FWHM of signal emitted by a 1 cm thick slab is 2 nm, and the corresponding angular width is 0.2° .

3. SCATTERING MATRIX AND SIGNAL LINE PROFILE FOR A SLAB WITH REFLECTING BOUNDARIES

The analysis developed above does not take into account reflection from the boundaries of nonlinear medium. It is clear that reflection gives rise to effects due to interference, which affects the scattered-wave line profile.

The pump, signal, and idler modes inside and outside a reflecting slab can be divided into forward and backward ones (propagating in the positive and negative directions along the z axis) (see Fig. 1). The forward and backward wave vectors associated with the same frequency differ only by the signs of their z -components. Wave vectors having equal magnitudes and opposite signs arise when signal and idler waves are incident upon the slab from both directions. Denote the forward ($K_{1z} > 0$) and backward ($K_{1z} < 0$) signal waves by subscripts 1 and 3, respectively, and the forward and backward idler waves by subscripts 2 and 4, respectively. The amplitude of each wave varies as the wave propagates across the slab because of parametric interaction. Additional variation of the amplitude is caused by absorption inside the slab and reflection from its boundaries. Linear scattering is neglected here. We denote the amplitudes of the forward and backward signal and idler waves leaving the slab by E_j ($j = 1, 2, 3, 4$), those of the incident waves by E_{j0} , and those propagating across the slab by $E_j(z)$.

The boundary conditions relating the amplitudes outside and inside the slab (at $z = \pm l/2$) can be represented as follows [20]:

$$\mathbf{A}' + \hat{\rho} \mathbf{A}'' = \hat{\tau} \mathbf{A}_0, \quad \mathbf{A} = \hat{\tau} \mathbf{A}'' + \hat{\rho}^* \mathbf{A}_0, \quad (19)$$

where

$$\mathbf{A}_0 \equiv \{A_{10}, A_{20}^*, A_{30}, A_{40}^*\}, \quad \mathbf{A} \equiv \{A_1, A_2^*, A_3, A_4^*\},$$

$$\mathbf{A}' \equiv \{A_1(-l/2), A_2^*(-l/2), A_3(l/2), A_4^*(l/2)\},$$

$$\mathbf{A}'' \equiv \{A_1(l/2), A_2^*(l/2), A_3(-l/2), A_4^*(-l/2)\}.$$

The elements of the diagonal matrix $\hat{\tau}$ are

$$\tau_1 = \tau_3 = t_1 \sqrt{\frac{n_1 \cos \vartheta_1}{\cos \theta_1}}, \quad \tau_2 = \tau_4 = t_2 \sqrt{\frac{n_2 \cos \vartheta_2}{\cos \theta_2}},$$

where t_1 and t_2 are the amplitude transmissivities characterizing the slab boundaries. The nonzero compo-

nents of the matrix $\hat{\rho}$ are

$$\rho_{13} = \rho_{31} \equiv \rho_1 \equiv r_1 e^{i\delta_1}, \quad \rho_{24} = \rho_{42} \equiv \rho_2 \equiv r_2 e^{-i\delta_2},$$

$$\delta_j \equiv |k_{jz}|l = \frac{\ln_j \omega_j}{c} \cos \vartheta_j,$$

where r_j denotes the amplitude reflectivities of the slab boundaries. Both r_j and t_j are calculated by using the Fresnel formulas [22]. If the optical density of the medium outside the slab is lower, then $r_j < 0$. When anisotropy is allowed for, the coefficients r_j and t_j depend both on the propagation direction of the incident waves and on their respective angles of incidence. Moreover, we may consider the effects due to birefringence, in which case each incident plane wave is associated with two forward and backward waves propagating across the slab. To simplify further analysis, we assume that the parametric interaction involves only signal and idler waves of definite polarization. We also assume that the orientation of the optical axes of the anisotropic layer is such that birefringence effects vanish and the polarizations of linearly polarized incident waves remain invariant after reflection and refraction at the slab boundary.

Reduced equations (9) relate both the forward waves $E_1(z)$ and $E_2(z)$ and the backward waves $E_3(z)$ and $E_4(z)$ pairwise. The only difference between the pairs is that the forward pump amplitude $E_0^{(+)}$ must be substituted into (9) to calculate $E_1(z)$ and $E_2(z)$, whereas the backward pump amplitude $E_0^{(-)}$ must be substituted to calculate $E_3(z)$ and $E_4(z)$. The incident pump amplitude is related to the amplitudes $E_0^{(+)}$ and $E_0^{(-)}$ inside the slab by the Airy formulas

$$E_0^{(+)} = \frac{t_0}{1 - r_0^2 \exp(2i\delta_0)} E_0,$$

$$E_0^{(-)} = \frac{t_0 r_0 \exp(i\delta_0)}{1 - r_0^2 \exp(2i\delta_0)} E_0 = r_0 \exp(i\delta_0) E_0^{(+)}.$$

Interaction between $E_1(z)$, $E_2(z)$, $E_3(z)$, and $E_4(z)$ in the presence of pumps $E_0^{(+)}$ and $E_0^{(-)}$ can be represented in terms of a general parametric interaction matrix as $\mathbf{A}'' = \hat{w} \mathbf{A}'$, where

$$\hat{w} = \begin{pmatrix} w_{11} & w_{12} & 0 & 0 \\ w_{21} & w_{22} & 0 & 0 \\ 0 & 0 & w_{11}^{(-)} & w_{12}^{(-)} \\ 0 & 0 & w_{21}^{(-)} & w_{22}^{(-)} \end{pmatrix}. \quad (20)$$

The elements w_{ij} ($i = 1, 2$) are identical with those of the parametric interaction matrix defined by (11) in the absence of reflection (after the change $E_0 \rightarrow E_0^{(+)}$).

The components $w_{ij}^{(-)}$ characterize interaction between the backward waves and are similar to w_{ij} , with the exception that E_0 is replaced by $E_0^{(-)}$ in expression (12) for β . The relation $\hat{w}^{(-1)} = \hat{w}(-l)$ means that the inverse matrix characterizes conversion of waves propagating in the negative direction along the z axis.

Combining (19) with (20), we find the scattering matrix \hat{U} for a slab:

$$\mathbf{A} = \hat{U} \mathbf{A}_0, \quad \hat{U} = \hat{t} \hat{w} (\hat{I} + \hat{\rho} \hat{w})^{-1} \hat{t} + \hat{\rho}^*. \quad (21)$$

Expressions for the elements of \hat{U} were presented in [20].

If neither signal nor idler wave is absorbed, then we have the condition

$$|U_{11}|^2 + |U_{13}|^2 - |U_{12}|^2 - |U_{14}|^2 = 1. \quad (22)$$

By the generalized Kirchhoff law (represented by (3)), the SPDC signal radiance in a slab that partially absorbs idler waves and partially reflects all waves is expressed as

$$N_{1'}^{\text{SPS}} = |U_{11}|^2 + |U_{13}|^2 = 1. \quad (23)$$

For PC of an idler input of radiance N_2 , we have

$$N_{1'} = N_{1'}^{\text{SPS}} + N_{1'}^{\text{PT}}, \quad N_{1'}^{\text{PT}} = |U_{12}|^2 N_2. \quad (24)$$

Instead of (15), we obtain the following expression for the SPDC signal intensity:

$$\begin{aligned} P_{\omega_1 \Omega_1}^{\text{SPS}} \Big|_{\substack{y_1=0 \\ y_2 \neq 0}} &= C_0 \frac{1 - R_1}{D_0 D_1 \tilde{D}_2} \{ \tilde{D}_2 (1 + R_0 R_1) g(\Delta, y_2) \\ &+ [\tilde{R}_2 (1 + R_0 R_1) (\cos 2\delta_2 - \tilde{R}_2) - 2r_0 r_1 \tilde{r}_2 (1 - \tilde{R}_2) \\ &\times \cos(\delta_0 + \delta_1) \cos \delta_2] g'(\Delta, y_2) \\ &- [\tilde{R}_2 (1 + R_0 R_1) \sin 2\delta_2 - 2r_0 r_1 \tilde{r}_2 (1 + \tilde{R}_2) \\ &\times \cos(\delta_0 + \delta_1) \sin \delta_2] g''(\Delta, y_2) \}. \end{aligned} \quad (25)$$

Here, the supplementary functions determining the

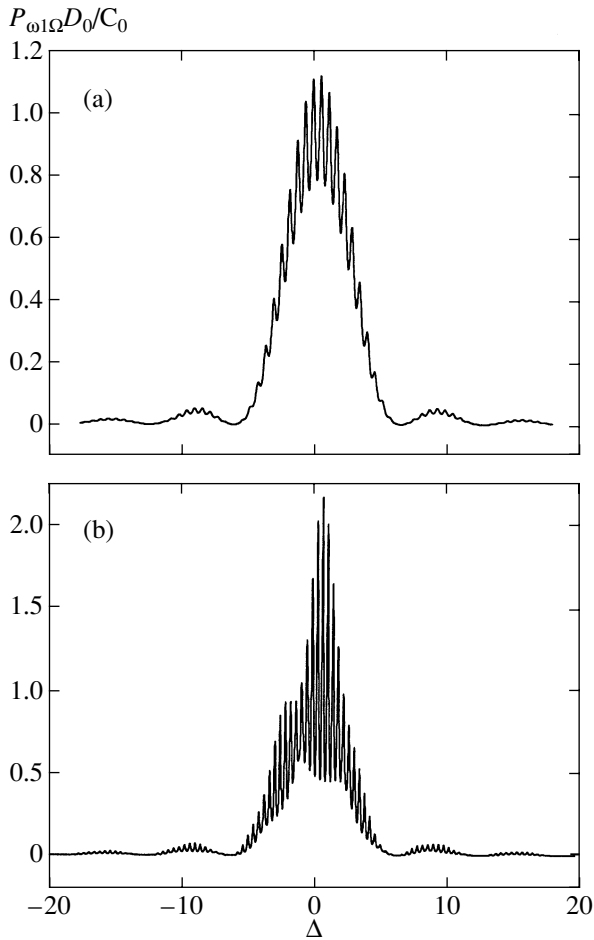


Fig. 2. SPDC line shape in a transparent slab that reflects signal waves ($r_1 = -0.3$): (a) other waves are not reflected; (b) idler and pump waves are reflected ($r_2 = -0.5$ and $r_0 = -0.5$).

form factor for scattered waves are

$$\begin{aligned}
 g'(\Delta, y_2) &\equiv \frac{4}{(\Delta^2 + y_2^2)^2} [(\Delta^2 - y_2^2) \\
 &\times (1 - \cosh y_2 \cos \Delta) - 2y_2 \Delta \sinh y_2 \sin \Delta], \\
 g''(\Delta, y_2) &\equiv \frac{4}{(\Delta^2 + y_2^2)^2} [(\Delta^2 - y_2^2) \sinh y_2 \sin \Delta \\
 &- 2y_2 \Delta (1 - \cosh y_2 \cos \Delta)], \\
 D_j &= 1 - 2R_j \cos 2\delta_j + R_j^2, \\
 \tilde{D}_j &= 1 - 2\tilde{R}_j \cos 2\tilde{\delta}_j + \tilde{R}_j^2,
 \end{aligned} \quad (26)$$

$R_j \equiv r_j^2$ is the reflection coefficient defined as the corresponding reflected-to-incident intensity ratio for a wave of frequency ω_j , $\tilde{R}_j \equiv \tilde{r}_j^2$, and $\tilde{r}_j \equiv r_j \exp(-y_j)$.

For a medium that is transparent at idler frequencies, but partially absorbs signal waves, an expression for SPDC intensity is derived from the generalized Kirchhoff law written represented by (4). Instead of (25), we obtain

$$\begin{aligned}
 P_{\omega_1, \Omega_1}^{\text{SPS}} \Big|_{\substack{y_1 \neq 0 \\ y_2 = 0}} &= C_0 \frac{(1 - R_1)(1 - R_2)}{D_0 \tilde{D}_1 D_2} F(\Delta, y_1, 0) \\
 &\times \{ 1 + R_2 + R_0 \tilde{R}_1 + R_0 \tilde{R}_1 R_2 \\
 &- 2r_0 \tilde{r}_1 r_2 [\cos(\Delta + 2\delta_0) + \cos \delta] \}.
 \end{aligned} \quad (27)$$

Here, the value of $\delta \equiv \delta_2 - \delta_1 - \delta_0$ differs from that of $\Delta \equiv \delta_2 + \delta_1 - \delta_0$.

In the case of arbitrary laws of wave absorption and reflection in the slab, the PC signal intensity is expressed as

$$\begin{aligned}
 P_{\omega_1, \Omega_1}^{\text{PT}} \Big|_{\substack{y_1 \neq 0 \\ y_2 \neq 0}} &= C_0 N_2 \frac{(1 - R_1)(1 - R_2)}{D_0 \tilde{D}_1 \tilde{D}_2} F(\Delta, y_1, y_2) \\
 &\times (1 - 2r_0 \tilde{r}_1 \tilde{r}_2 \cos \delta + R_0 \tilde{R}_1 \tilde{R}_2).
 \end{aligned} \quad (28)$$

It is obvious that the PC line profile in the presence of reflections differs from the SPDC line profile in the absence of both absorption at signal frequencies (cf. (25) and (28)) and appreciable absorption at idler frequencies (cf. (27) and (28)).

Reflections in a slab give rise to fine interference structure in SPDC and PC line profiles. When the crystal is transparent, the modulation due to frequency- or angle-dependent variation of $\text{sinc}^2(\Delta/2)$ combines with additional modulation of two types. One of these is associated with the behavior of terms containing $2\delta_1$ and $2\delta_2$. Moreover, these factors characterize the Airy linear interference of signal and idler waves in a slab. Interference of this kind occurs when the superposition of incident and reflected waves of each particular frequency is independent of the presence of other waves. This interference manifests itself in spectra associated with nonlinear interaction as well. It leads to double periodic modulation of spectra with periods determined by the conditions $d_j = \pi n$, where n is an integer. The corresponding modulation depth is determined by the reflection coefficients R_1 and R_2 .

Figure 2a shows an example of frequency-dependent SPDC line profile in the case of Airy linear interference between reflected signal waves when $R_2 = 0$. Whether the pump is reflected or not, the SPDC line profile remains invariant. The relation between the Airy modulation period and the modulation controlled by the function $\text{sinc}^2(\Delta/2)$ is determined by specific parameters of the medium. The SPDC signal intensity concentrates within the principal maximum of

1 $\text{sinc}^2(\Delta/2)$, i.e., within the frequency bandwidth given, as in a nonreflecting slab, by the expression

$$\Delta\omega_{1s} \equiv \frac{\int P_{\omega_1, \Omega_1} d\omega_1}{P_{\omega_1, \Omega_1}} \quad (29)$$

$$= \frac{2\pi \cos(\vartheta_2 - \vartheta_0)}{|u_2^{-1} - u_1^{-1} \cos(\vartheta_1 - \vartheta_2)|l},$$

where u_m denotes group velocities in the crystal. To observe extra peaks in the frequency profile of a scattered-wave line, we must have the condition $\Delta\omega_{ml} < \Delta\omega_{1s}$, where $\Delta\omega_{ml} = \pi u_m / l \cos \vartheta_m$ is the frequency spacing between the peaks due to linear interference of signal or idler waves. Analogous relations for angular intervals determine the observability of Airy interference in the angular SPDC line profile. For example, when parametric interaction of the type considered at the end of the preceding section takes place inside a 1 cm thick slab of KDP crystal, the modulation period associated with wave interference varies between 0.013 and 0.014 nm, whereas the spectral width of the principal maximum is substantially larger (0.5 nm). The corresponding period of interference modulation in the angular line profile is similar to the angular width of the principal maximum.

The other type of SPDC line profile modulation, due to wave reflection in the slab, is of greater interest. Modulation of this type is associated with change in the combination of parameters δ_j :

$$\Delta + 2\delta_0, \quad \delta, \quad 2(\delta_2 - \delta_1) \equiv 2(\delta + \delta_0),$$

$$2(\delta_1 + \delta_2) \equiv 2(\Delta + \delta_0).$$

It can be observed only when both signal and idler waves are reflected by the boundaries. Note that the reflected pump wave somewhat changes the overall intensity distribution, but it is not required to observe interference. The peaks associated with changes in the mismatch δ by multiples of π (which is equivalent to changes in $\delta_1 - \delta_2$ by multiples of π) are spaced approximately as the Airy interference maxima. For example, the inverse frequency widths of the Airy maxima, $\Delta\omega_{ml}$ and $\Delta\omega'_1$, satisfy the relation

$$(\Delta\omega'_1)^{-1} = (\Delta\omega_{1l})^{-1} + (\Delta\omega_{2l})^{-1}. \quad (30)$$

However, the occurrence of the peaks associated with changes by multiples of π in the mismatch $\Delta + 2\delta_0$ and, therefore, in $\delta_2 + \delta_1$ (if δ_0 is constant) is strictly related to the initial mismatch. Interference of this type can be classified as nonlinear, because the locations of the peaks depend on the phases of all waves involved in a parametric interaction. The frequency bandwidth due to the nonlinear interference associated with the phase

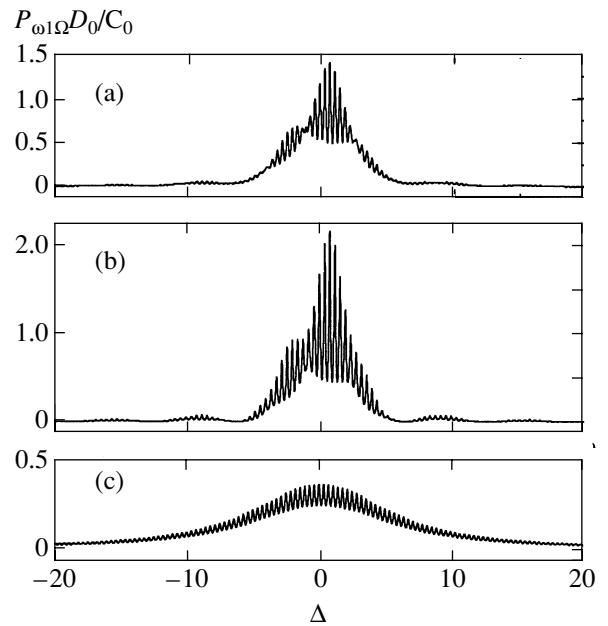


Fig. 3. SPDC line shape in a reflecting slab ($r_0 = -0.5$, $r_1 = -0.3$, $r_2 = -0.5$) for several values of absorption coefficients at signal and idler frequencies: (a) $\alpha_1 l = 0$, $\alpha_2 l = 1$; (b) $\alpha_1 l = 1$, $\alpha_2 l = 0$; (c) $\alpha_1 l = 0$, $\alpha_2 l = 10$.

incursion $2(\delta_1 + \delta_2) \equiv 2(\Delta + \delta_0)$ is determined by the relation

$$(\Delta\omega_{1nl})^{-1} = |(\Delta\omega_{1l})^{-1} - (\Delta\omega_{2l})^{-1}|. \quad (31)$$

The corresponding modulation period is smaller than the frequency width of the central maximum of $\text{sinc}^2(\Delta/2)$ by a factor of four. The period of the nonlinear interference associated with the phase incursion $\Delta + 2\delta_0$ is smaller than the frequency width of the same central maximum by a factor of two. Figure 2b shows an example of frequency-domain scattered-wave line profile observed in the case when the signal, idler, and pump waves are reflected from the boundaries. It demonstrates that nonlinear interference leads to periodic variation of the amplitude of high-frequency modulation of the spectrum.

Nonlinear interference is caused by parametric interaction between forward and backward waves and linear interference between signal waves of frequency ω_1 . Similar effects were observed, for example, in studies of frequency-angular intensity distribution and correlation between SPDC signal and idler channel intensities in slabs of nonlinear crystal separated by layers of an optically linear medium [23–26].

Figure 3 illustrates the influence of the signal and idler waves on the interference pattern observed at the signal frequency. With increasing absorption, the luminous efficiency of the interference pattern, which is determined by linear and nonlinear interference of the absorbed wave, decreases. The variation of luminous

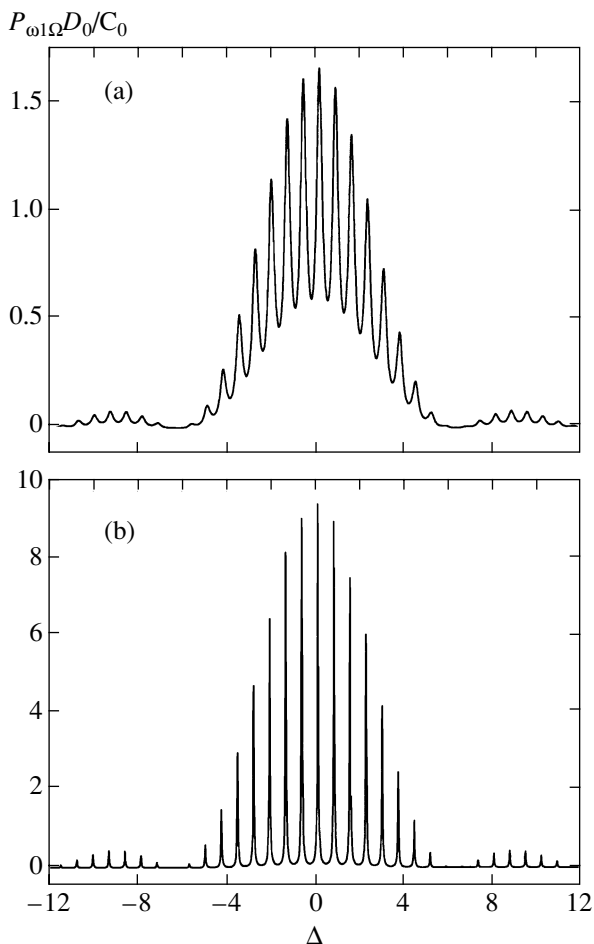


Fig. 4. SPDC line shape for a slab that reflects only idler waves ($r_0 = r_1 = 0$): (a) $r_2 = -0.5$, (b) $r_2 = -0.9$.

efficiency concurs with analogous variations of the basic line profile, which are characteristic of the slab in the absence of absorption. The increase in absorption at both frequencies leads to gradual decrease in contrast, and the interference structure of the line profile is eventually blurred out. The effects of reflection on the SPDC line profile can be observed experimentally only under certain conditions. These conditions are generally violated when SPDC is used in spectroscopy, but this does not preclude determination of volume-averaged values of refractive index and absorption coefficient at idler frequencies from smoothed scattered-wave line profiles. Reflection effects must be taken into account in measurements of integral scattered-wave intensity. For example, this is required when SPDC is used in photometry [20, 27–29].

4. INTERFERENCE OF ELECTROMAGNETIC ZERO-POINT FLUCTUATIONS OF THE VACUUM

Consider SPDC in the case when the idler wave is reflected by the slab boundaries, whereas the signal and

pump are not. Suppose that the idler wave can be absorbed. Figure 4 shows the frequency-domain line profiles corresponding to several values of the absorption coefficient r_2 . It is clear that the overall signal line profile is modulated. The modulation frequency and depth are described by the Airy linear interference for idler (rather than signal) waves.

Generally, the efficiency of each act of parametric conversion depends, among other factors, on the average values of field operators in the input idler and signal modes [10]. In SPDC observations, only the pump wave is incident on the crystal. The thermal population of the modes is too low to ensure the required scattering efficiency. In this case, the role of seed is played only by the so-called electromagnetic zero-point fluctuations of the vacuum at the idler frequency when a signal wave is detected or at the signal frequency when an idler wave is detected. Recall that the effective radiance of zero-point fluctuations of the vacuum in PC processes is one photon per mode [30]. If the seed is an external free wave “separated” from its source, then its intensity inside the crystal will depend on the absorption and reflection coefficients of the medium at the idler frequency and therefore affect the signal spectrum. In SPDC, idler waves are generated only via decay of the pump. The “free” idler wave is then reflected by the slab boundaries and absorbed as it propagates through the medium. In the linear-amplification approximation, the emerging idler wave weakly interacts with the pump and feedback is negligible. Therefore, the idler wave does not affect the signal spectrum, and the line profile shown in Fig. 4 must not be sensitive to the intensity distribution of the idler wave generated in the medium. Thus, the signal line profile shown here is due only to the field fluctuations at the idler frequency, which participate initially in each elementary act of scattering and subsequently in the interference of the signal waves originating from different points in a nonlinear medium. The interference structure of the signal line with parameters determined by the idler-frequency properties of the crystal can be attributed to interference with zero-point fluctuations of the vacuum [31].

The interference pattern in line profile or signal–idler intensity cross-correlation function reflects the spatial distribution of the vacuum states of the field in the slab. Spatial nonuniformity must be taken into account in a comprehensive quantum-theoretic analysis of the problem even at the stage of field quantization. To perform quantization, the operator of field strength in an individual mode is represented as follows [32]:

$$E_j(\mathbf{r}, t) = v_j(\mathbf{r})a_j(t) + v_j^*(\mathbf{r})a_j^\dagger(t), \tag{32}$$

where $a_j^\dagger(t) = a_j^\dagger \exp(i\omega_j t)$ and $a_j(t) = a_j \exp(-i\omega_j t)$ are the j th-mode photon creation and annihilation operators, respectively, and $v_j(\mathbf{r})$ is an eigenfunction of the

corresponding boundary value problem for the spatial field distribution described by Maxwell's equations and medium-specific boundary conditions. It is obvious that every j th-mode field has the same spatial distribution irrespective of its state, which may be a Fock-space state with a constant number of photons, a mixed or vacuum one, etc. When the slab has reflecting boundaries, an interference pattern corresponding to $v_j(\mathbf{r})$ is observed, and similar patterns are characteristic of both single-mode equilibrium thermal field and vacuum-state field. Since both signal and idler input fields are in the vacuum state in SPDC, the signal spectrum exhibits an interference structure associated with the vacuum states of the field at the idler frequency. A different state of the field added to input in the idler channel can change the frequency-domain line profile of the scattered wave. However, the change will occur only when all modes are populated nonuniformly, i.e., when the mode occupation number (mean number of photons in a mode) varies from mode to mode because of the additional field. Otherwise, the signal line profile will be similar to that due to the interference of zero-point fluctuations of the vacuum described here.

If R_0 , R_1 , and y_2 in (25) are assumed to be small, this expression describes light scattering by interference polaritons [33] in those spectral regions where the contribution of the Raman tensor to the scattered-wave intensity is negligible. The contribution to light scattering by polaritons due to parametric processes is the main source of signal in spectral regions far from phonon resonances when the difference of idler and phonon wavenumbers (measured in cm^{-1}) is greater than the phonon decay constant. The curves connecting the interference peaks of the same order $m = \delta_2/\pi = k_{2z}l/\pi$ can be used to measure the dispersion of interference polaritons. As $R_2 \rightarrow 1$, the conditions for total reflection of the polariton waves trapped in the slab are satisfied. In this case, peaks in the fine signal-profile structure correspond to scattering by waveguide polaritons [33–35]. For example, this is characteristic of parametric interaction in lithium niobate crystals, when the idler wave corresponds to the upper polariton branch with wavenumbers about 2000 cm^{-1} . In this case, observation of linear interference of zero-point fluctuations of the vacuum requires either a receiver with a sufficiently high resolution or a sufficiently thin crystal film, because the spacing between the lines is 0.2 cm^{-1} and 4 cm^{-1} for 1 cm and $500 \mu\text{m}$ thick slabs.

5. SCATTERING MATRIX AND SIGNAL LINE PROFILE IN MEDIA WITH SPATIALLY MODULATED SECOND-ORDER SUSCEPTIBILITY

We consider three-wave parametric interaction in a specimen of a layered medium with second-order susceptibility varying in one direction. First, we suppose that the value of $\chi^{(2)}$ varies periodically. We assume that

the spatial modulation of linear susceptibility so weak that the effects due to variation of refractive index and absorption coefficient can be neglected. This approximation is valid, for example, in analysis of parametric processes in ferroelectric crystals with regular domain structure [1, 3, 4, 6–9]. In such crystals, a change in the sign of spontaneous polarization between domains is associated with a change in all even-order susceptibilities in the expansion of polarizability in powers of field strength, while the susceptibilities of odd order remain invariant [36].

Periodically varying second-order susceptibility can be represented as the Fourier series

$$\chi^{(2)}(\mathbf{r}) = \sum_{m=-\infty}^{\infty} \chi_m^{(2)} \exp(i\mathbf{q}_m \cdot \mathbf{r}) \quad (33)$$

with spatial-harmonic amplitudes

$$\chi_m^{(2)}(\mathbf{r}) = \frac{1}{d} \int_{-d/2}^{d/2} \chi^{(2)}(\mathbf{r}) \exp(-i\mathbf{q}_m \cdot \mathbf{r}) d\mathbf{r}, \quad (34)$$

where d is the period of a one-dimensional “nonlinear superlattice” (modulation period) and $\mathbf{q}_m = \mathbf{q}m$ denotes vectors of the reciprocal superlattice, with an integer m and $\mathbf{q} \equiv (2\pi/d)\mathbf{n}$ (\mathbf{n} is the unit normal vector to the layer boundaries). In the approximation considered here, the input amplitudes of forward waves are continuous across the boundary of the medium, and the scattering matrix is identical to the matrix of the parametric interaction of forward waves. The nonlinear polarization at the frequency ω_1 is expressed as

$$\begin{aligned} P_1(\omega_1 = \omega_0 - \omega_2) \\ = \sum_{m=-\infty}^{\infty} \chi_m^{(2)} E_0 E_2^* \exp[i(\mathbf{k}_0 - \mathbf{k}_2 + \mathbf{q}_m) \cdot \mathbf{r}]. \end{aligned} \quad (35)$$

The nonlinear polarization at the frequency ω_2 is given by a similar expression. The corresponding reduced equations are

$$\frac{dE_1(z)}{dz} + i \sum_m \sigma_{1m} E_0 E_2^*(z) \exp\left(-\frac{i\Delta_m z}{l}\right) + \frac{y_1}{l} E_1(z) = 0, \quad (36)$$

$$\frac{dE_2(z)}{dz} + i \sum_m \sigma_{2m} E_0 E_1^*(z) \exp\left(-\frac{i\Delta_m z}{l}\right) + \frac{y_2}{l} E_2(z) = 0.$$

Here, the z axis is aligned with the normal to the nonlinear layers,

$$\Delta_m \equiv l(k_{1z} + k_{2z} - k_{0z} - q_m) \equiv \delta_1 + \delta_2 - \delta_3 - q_m l$$

is the dimensionless wave-vector mismatch for the m th harmonic, Δ_m/l differs from the mismatch Δ/l in a spatially uniform medium by the magnitude of the reciprocal-superlattice vector q_m , and

$$\sigma_{jm} \equiv 2\pi\chi_m\omega_j/cn_j\cos\vartheta \quad (j = 1, 2).$$

When the PC coefficient is small, the absolute values of the parameters $\beta_{1m} \equiv i\sigma_{1m}E_0l$ and $\beta_{2m} \equiv -i\delta_{2m}^*E_0l$ characterizing the efficiency of wave interaction in the slab are small: $|\beta_m| = \sqrt{\beta_{1m}\beta_{2m}} \ll 1$. The parameter β_m is defined by analogy with the parameter β for a homogeneous medium (see (12)), with $\chi^{(2)} \rightarrow \chi_m^{(2)}$.

The solution of Eq. (36) determines the elements of the scattering matrix, which is identical to the parametric interaction matrix for waves in the layered medium considered here. In the linear-amplification approximation (up to terms of order β_m^2),

$$\begin{aligned} w_{11} &\approx \exp(-y_1) + \sum_{m=-\infty}^{\infty} |\beta_m|^2 f_1(\eta_m) \\ &+ \sum_{m=-\infty}^{\infty} \sum_{\substack{m'=-\infty \\ m' \neq m}}^{\infty} \beta_{1m}\beta_{2m'} \frac{\exp(\eta_m - \eta_{m'} - y_1)}{2\eta_{m'}} \\ &\times [\varphi(\eta_m) - \varphi(\eta_m - \eta_{m'})], \\ w_{12} &\approx \sum_{m=-\infty}^{\infty} i\beta_m f(\eta_m), \end{aligned} \quad (37)$$

where

$$\varphi(x) \equiv \frac{e^{-2x} - 1}{2x}.$$

The functions $f(\eta_m)$ and $f_1(\eta_m)$ are defined by (14) with the replacements $\Delta \rightarrow \Delta_m$ and $\eta \rightarrow \eta_m \equiv (-y_1 + y_2 + i\Delta_m)/2 = \eta - imq_z l$:

$$\begin{aligned} f_1(\eta_m) &\equiv \frac{1}{(2\eta_m)^2} \\ &\times [\exp(-y_2 - i\Delta_m) - (1 - 2\eta_m)\exp(-y_1)] \\ &= \frac{\exp(-y_1)[\varphi(\eta_m) + 1]}{2\eta_m}, \\ f(\eta_m) &\equiv \frac{1}{2\eta_m} \left[\exp\left(-y_2 - \frac{i\Delta_m}{2}\right) \right. \\ &\left. - \exp\left(-y_1 + \frac{i\Delta_m}{2}\right) \right] = \exp\left(-y_1 + \frac{i\Delta_m}{2}\right) \varphi(\eta_m). \end{aligned} \quad (38)$$

In (37), the element w_{12} contains contributions of all spatial harmonics $\chi_m^{(2)}$, which are similar to the expression for a homogeneous specimen (cf. (37) and (13)), but with $\Delta \rightarrow \Delta_m$ and $\chi^{(2)} \rightarrow \chi_m^{(2)}$. The expression for w_{11} contains additional summands corresponding to interference of the contributions due to different harmonics $\chi_m^{(2)}$ and $\chi_{m'}^{(2)}$ ($m \neq m'$).

When the idler wave is absorbed, the generalized Kirchhoff law dictates the following expression for the signal intensity $P_{\omega_1\Omega_1}$ in SPDC:

$$\begin{aligned} P_{\omega_1\Omega_1} &= C \sum_{m=-\infty}^{\infty} |\chi_m|^2 g(\Delta_m, y_2) \\ &+ C \sum_{m=-\infty}^{\infty} \sum_{\substack{m'=-\infty \\ m' \neq m}}^{\infty} (-1)^{n(m'-m)} \chi_m^* \chi_{m'} \\ &\times \left[\frac{\exp(-i\Delta - y_2) - 1}{(y_2 + i\Delta - imq_z l)(y_2 + i\Delta - im'q_z l)} \right. \\ &\left. \times \frac{\exp(i\Delta - y_2) - 1}{(y_2 - i\Delta - imq_z l)(y_2 - i\Delta - im'q_z l)} \right]. \end{aligned} \quad (39)$$

Here, the coefficient is equal to C_0/χ^2 for a homogeneous medium (see (15), (16), (25)–(28)) and n is the number of periods spanned by the thickness l ($n \equiv l/d$). The scattered-wave line profile in a periodically modulated medium is characterized by two terms. One of them is the sum of contributions of individual harmonics. In each summand, the intensity distribution relative to the maximum is similar to that in a homogeneous medium (function $g(\Delta, y_2)$ in (15)). For each component, the new maxima are shifted according to the quasi-matching condition $\Delta(w_1, \theta_1) = -q_m l \equiv -2\pi mn$. The value of each summand is proportional to the squared amplitude of the corresponding harmonic. The other term in (39) contains products of different harmonics $\chi_m^{(2)}$ and describes their interference.

When neither signal nor idler wave is absorbed, the SPDC intensity is

$$P_{\omega_1\Omega_1} \Big|_{y_1=0, y_2=0} = C \left| \sum_{m=-\infty}^{\infty} \chi_m \operatorname{sinc}\left(\frac{\Delta_m}{2}\right) \right|^2. \quad (40)$$

Figure 5 shows examples of SPDC intensity versus phase mismatch $\Delta k/q$ calculated by using (40) in the simplest case of meander-type periodic distribution of $\chi^{(2)}(z)$. This distribution is characteristic of multidomain crystals in which the sign of second-order nonlinear susceptibility sharply reverses across the domain

boundaries and the transition-layer thickness is negligible as compared to the thickness of a domain of either sign. In this case, (40) yields the following expression for the SPDC line profile:

$$P_{\omega_1, \Omega_1} \Big|_{\substack{y_1=0 \\ y_2=0}} = C \bar{\chi}^2 \frac{\text{sinc}^2(\Delta/2)}{\sin^2(\Delta/2n)} \times \left(1 - 2 \cos \frac{\rho \Delta}{2n} \cos \frac{\Delta}{2n} + \cos^2 \frac{\Delta}{2n} \right),$$

where $\rho \equiv (l_1 - l_2)/d$ is a parameter characterizing the asymmetry of the domain system ($d = l_1 + l_2$ is the superlattice period). Both spectral and angular spacings between the peaks due to nonlinear diffraction increase with decreasing superlattice period. Unlike the widths of the peaks, they are independent of the total thickness of a specimen. For example, consider collinear parametric interaction of *ooe* type in a lithium niobate crystal with regular domain structure and domain walls parallel to the *xz* crystallographic plane. For this configuration, the difference between the curves corresponding to zeroth- and first-order quasi-matching is about 100 cm^{-1} if the domain layer thickness is $5 \text{ }\mu\text{m}$. Accordingly, the difference is smaller by an order of magnitude if the thickness is $500 \text{ }\mu\text{m}$. These values are obtained for a 488-nm pump propagating in the crystallographic planes *yz* of domains at an angle of 57° , crossing the domain walls. In this case, collinear interaction is observed when the signal wavelength is about 510 nm .

Expression (40) for signal intensity contains the amplitudes $|\chi_m^{(2)}|$ and phases φ_m of the spatial harmonics $\chi_m^{(2)} \equiv |\chi_m^{(2)}| \exp(i\varphi_m)$ (which are complex-valued in the general case). When the imaginary part of $\chi^{(2)}(\mathbf{r})$ vanishes (far from the resonances of the medium), it holds that

$$\chi_m^{(2)} = (\chi_{-m}^{(2)})^*, \quad |\chi_m^{(2)}| = |\chi_{-m}^{(2)}|, \quad \varphi_m = -\varphi_{-m}.$$

The direct relation between SPDC spectrum and spatial distribution of second-order susceptibility can be used as a basis for measuring $\chi^{(2)}(\mathbf{r})$ in layered spatially non-uniform crystals and nonlinear structures. Measuring the ratio of the peak intensities associated with nonlinear diffraction in different orders of quasi-matching, for which $|\Delta| = 2\pi mn$, one can find the ratio of different harmonic amplitudes $|\chi_m^{(2)}|$. Since the interference terms directly depend on the phases φ_m , the signal intensity is redistributed among the quasi-matching maxima when $\Delta \neq 2\pi mn$. The interference is most pronounced in scat-

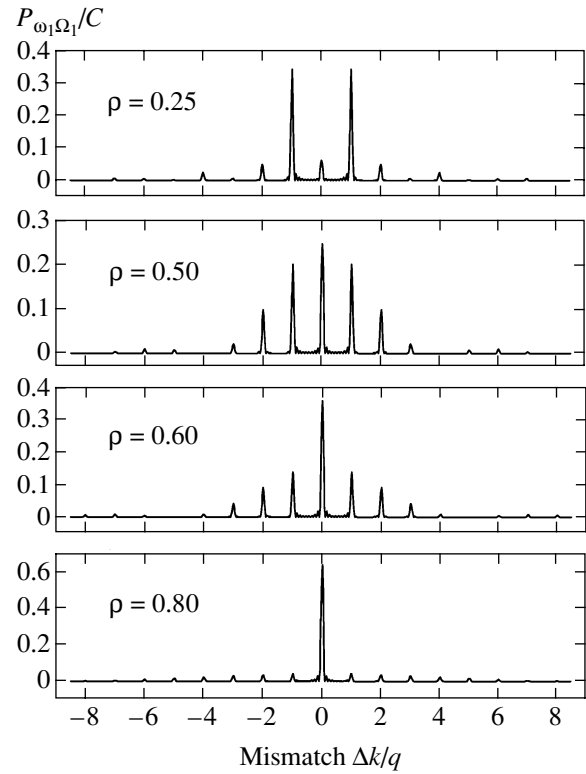


Fig. 5. SPDC line shape in a transparent ferroelectric with regular domain structure for different domain thickness ratios.

tering by specimens spanning just a few superlattice periods.

When the idler wave is absorbed, each peak associated with nonlinear diffraction is broadened, but not shifted (see Fig. 6). If the number of domains is so large that $n \gg y_2/n$, then (39) reduces to

$$P_{\omega_1, \Omega_1} = 2C_0 y_2 \sum_{m=-\infty}^{\infty} \frac{|\chi_m^{(2)}|^2}{y_2^2 + (\Delta - 2\pi mn)^2}. \quad (41)$$

The width of each nonlinear-diffraction peak on the scale of Δ is determined by the integral absorption y_2 over the entire crystal thickness nd , whereas information about the phases φ_m is lost. Nevertheless, the nonlinear-diffraction bands can be observed if the absorption over a superlattice period, y_2/n , is relatively weak. For example, if the domain size measured along the idler-wave direction does not exceed $5 \text{ }\mu\text{m}$, then the diffraction pattern can be observed in the range of idler frequencies such that $\alpha_2 \leq 2000 \text{ cm}^{-1}$. Conversely, if absorption is so strong that $y_2/n \gg 1$, then the nonlinear-diffraction bands are blurred out and the line of a parametrically scattered wave is a single broad Lorentzian curve centered at $\Delta = 0$. In the latter case, even the values of $|\chi_m^{(2)}|$ cannot be measured.

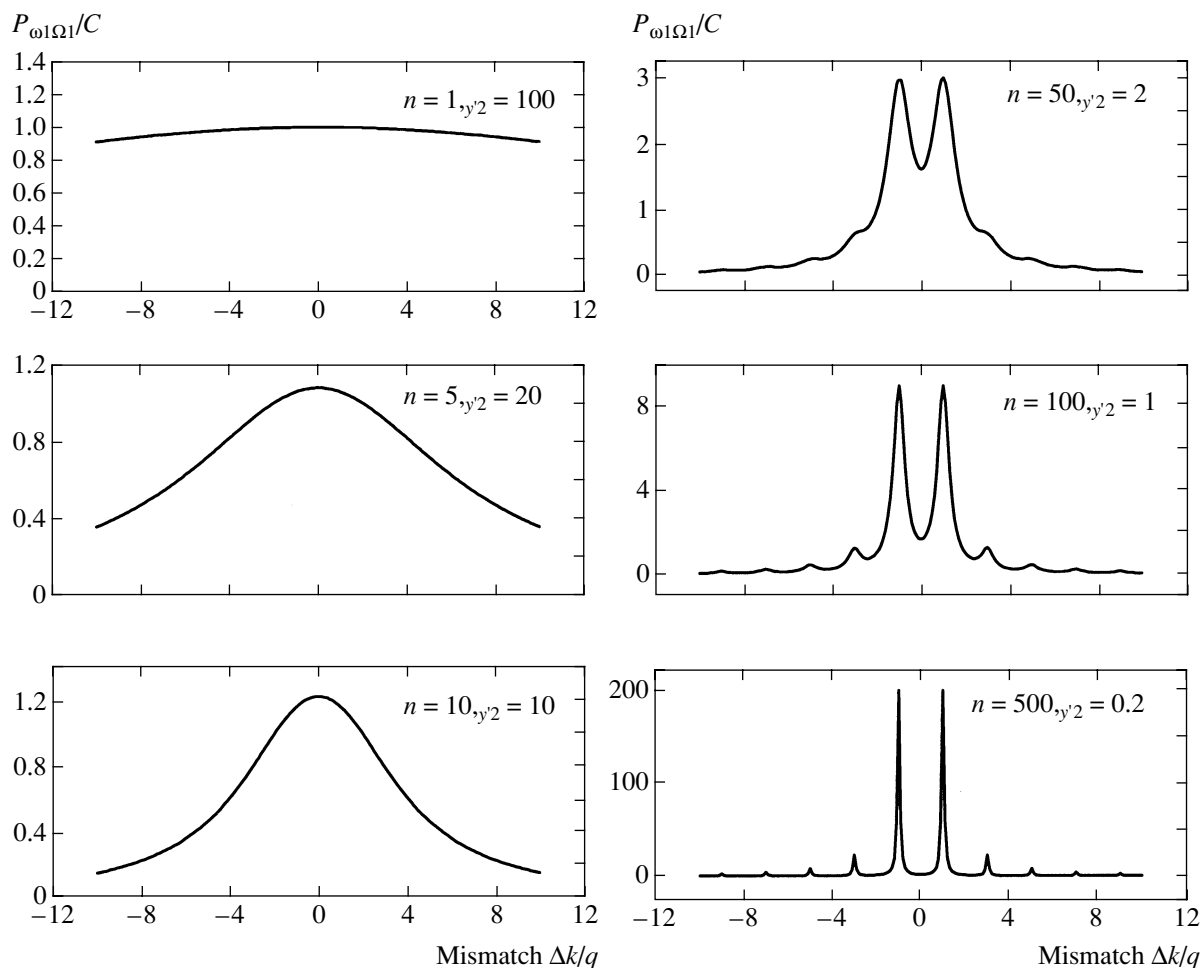


Fig. 6. —????????????????

2

SPDC spectra can also be used to measure the complete profile $\chi^{(2)}(z)$ in a weakly absorbing specimen of thickness l with an arbitrary distribution of second-order susceptibility. Consider the situation when the specimen is a part of a periodic medium in which the period of $\chi^{(2)}(z)$ is equal to l . If the pump occupies only a slab $\{-l/2, l/2\}$ in the medium, then the parametrically scattered signal is identical to that generated by a specimen of thickness l . The corresponding SPDC intensity distribution is described by (39) and (40) with $n = 1$ and

$$\chi_m = \frac{1}{l} \int_{-l/2}^{l/2} \chi^{(2)}(z) \exp\left(-i\frac{2\pi m}{l}z\right) dz. \quad (42)$$

In principle, the inverse problem of reconstruction of a complete profile $\chi^{(2)}(z)$ can be solved by using any three-wave parametric process, including stimulated up-conversion, second-harmonic generation, and cascade processes [3, 4, 6–9]. However, when using a stimulated process, one always has to deal with insufficient or nonuniform population of the converter modes

induced by input radiation. For example, the line profile of parametric conversion determined by the scattering matrix elements w_{12} is generally expressed as

$$P(\omega_1, \theta_1) = P(\omega_2, \theta_2) \frac{\omega_1^3 \cos \theta_1}{\omega_2^3 \cos \theta_2} |w_{12}|^2 = CN(\omega_2, \theta_2) \left| \sum_{m=-\infty}^{\infty} \chi_m f(\eta_m) \right|^2, \quad (43)$$

where $N(\omega_2, \theta_2)$ is the distribution of the photon number in the input idler mode, whereas strictly uniform population of input idler modes is guaranteed (by virtue of zero-point fluctuations of the vacuum) when spontaneous SPDC is used in the linear-amplification approximation. Information about domain structure can also be obtained by measuring a line profile even under the simplest conditions, when the effects due to interference are negligible. The number and relative intensity of shifted curves can be used to find the number of spa-

tial harmonics and the relative values of $|\chi_m^{(2)}|_2$; the shift direction and spacing between the parametric curves, to determine the direction and period of variation of second-order nonlinear susceptibility [9, 37–40].

6. CONCLUSIONS

In this study, we describe frequency-angular distributions for spontaneous parametric down-conversion and parametric conversion by applying a general approach based on the scattering matrix and the generalized Kirchhoff law. This approach makes it possible to solve a problem in quantum optics without invoking the formal procedure of field quantization for the spatially nonuniform nonlinear medium consisting of a nonlinear crystal and the surrounding space. The eigenfunctions of the corresponding wave problem describing a spatial distribution governed by Maxwell's equations subject to boundary conditions are not required. The elements of the scattering matrix are calculated for classical waves and then used as coefficients relating the quantum operators of input and output waves. The approach relies on the similarity between Maxwell's equations for classical fields and the Heisenberg equations for field operators in free space. Thus, intensity distributions can be obtained both for classical down-converted signals and for signals of essentially quantum nature generated via scattering of a pump by electromagnetic zero-point fluctuations of the vacuum.

Even though the generalized Kirchhoff law allows one to ignore the spatial distribution of modes in calculations, it can be used to obtain correct spatial and spectral distributions of scattered-wave intensity. In particular, we have obtained expressions for SPDC involving interference and waveguide polaritons without using the spatial dependence of the wavefunctions describing the corresponding states of the field in a slab. The calculated SPDC line profiles reflect the behavior of $v_m(\mathbf{r})$ for eigenmodes in spatially nonuniform media, including crystalline slabs characterized by absorption, semi-transparent boundaries, and nonuniformly distributed second-order susceptibility. In addition to its convenience, an important advantage of the approach based on the generalized Kirchhoff law is the possibility to allow for absorption of signal or idler waves. As in formulations of fluctuation-dissipation theorems, absorption is taken into account on a phenomenological level. The distinction is that the generalized Kirchhoff law deals with directly measurable characteristics: correlation functions of input and output fields.

It should be noted that the use of the generalized Kirchhoff law in the calculation of the line profile for a stimulated difference-frequency signal reduces to a standard classical calculation of the input field intensity based on the scattering-matrix elements relating the input and output fields. Expressions (16), (28), and (43) for the line profile for a stimulated difference-frequency signal generated in a layered inhomogeneous

medium are obtained directly by solving the reduced equations for slowly varying field amplitudes. Analogous equations describe both sum-frequency (in particular, second-harmonic) generation and each three-wave stage of stimulated cascade processes of higher orders. The only difference lies in the definitions of wave-vector mismatch Δ and parameter δ_i for sum-frequency generation: the signal and idler wave vectors must be taken with opposite signs.

Analysis of SPDC intensity spectrum can serve as a basis for measuring spatial variations of linear and nonlinear optical susceptibilities. One advantage is that SPDC has a very broad spectrum determined by the spectrum of zero-point fluctuations of the vacuum, whereas the signal spectrum in any stimulated frequency-conversion process is restricted to the spectrum of incident radiation. Note also that the method based on SPDC makes it possible to examine domain structures lying in the bulk of a crystal, man-made layered structures, and photonic crystals. The results presented here can be applied to measure one-dimensional distributions of $\chi^{(2)}$ in media with vanishingly small variations of linear susceptibility. The approach based on the generalized Kirchhoff law can be extended to media with nonuniform nonlinearities characterized by arbitrary irregular distributions of refractive indices and absorption coefficients.

ACKNOWLEDGMENTS

This work was supported by the Russian Foundation for Basic Research, project nos. 02-02-16843 and 03-02-16364 and by grant NSh-166.2003.02 under the Program of State Support of Leading Scientific Schools.

REFERENCES

1. A. V. Golenishchev-Kutuzov, V. A. Golenishchev-Kutuzov, and R. I. Kalimullin, *Usp. Fiz. Nauk* **170**, 697 (2000) [*Phys.-Usp.* **43**, 647 (2000)].
2. G. D'Aguzzo, M. Centini, M. Scalora, *et al.*, *Phys. Rev. E* **64**, 016 609 (2001).
3. R. L. Byer, *J. Nonlinear Opt. Phys. Mater.* **6**, 549 (1997).
4. D. K. Serkland, M. M. Fejer, R. L. Byer, and Y. Yamamoto, *Opt. Lett.* **20**, 1649 (1995).
5. M. Scalora, M. J. Bloemer, A. S. Manka, *et al.*, *Phys. Rev. A* **56**, 3166 (1997).
6. N. V. Kravtsov, G. D. Laptev, I. I. Naumova, *et al.*, *Kvantovaya Élektron. (Moscow)* **32**, 923 (2002).
7. A. C. Chirkin, V. V. Volkov, G. D. Laptev, and E. Yu. Morozov, *Kvantovaya Élektron. (Moscow)* **30**, 847 (2000).
8. S. G. Grechin and V. G. Dmitriev, *Kvantovaya Élektron. (Moscow)* **26**, 151 (1999).
9. G. Kh. Kitaeva, A. A. Mikhaïlovskii, and A. N. Penin, *Zh. Éksp. Teor. Fiz.* **112**, 2001 (1997) [*JETP* **85**, 1094 (1997)].
10. D. N. Klyshko, *Photons and Nonlinear Optics* (Nauka, Moscow, 1980).

11. D. N. Klyshko, *Izv. Akad. Nauk SSSR, Ser. Fiz.* **46**, 1478 (1982).
12. D. N. Klyshko, *Zh. Éksp. Teor. Fiz.* **55**, 1006 (1968) [*Sov. Phys. JETP* **28**, 522 (1968)].
13. D. N. Klyshko, *Pis'ma Zh. Éksp. Teor. Fiz.* **6**, 490 (1967) [*JETP Lett.* **6**, 23 (1967)].
14. D. N. Klyshko, *Physical Fundamentals of Quantum Electronics* (Nauka, Moscow, 1986).
15. D. N. Klyshko, *Zh. Éksp. Teor. Fiz.* **83**, 1313 (1982) [*Sov. Phys. JETP* **56**, 753 (1982)].
16. D. N. Klyshko, *Usp. Fiz. Nauk* **166**, 613 (1996) [*Phys.–Usp.* **39**, 573 (1996)].
17. D. N. Klyshko, A. N. Penin, and B. F. Polkovnikov, *Pis'ma Zh. Éksp. Teor. Fiz.* **11**, 11 (1970) [*JETP Lett.* **11**, 5 (1970)].
18. D. N. Klyshko, V. F. Kutsov, A. N. Penin, and B. F. Polkovnikov, *Zh. Éksp. Teor. Fiz.* **62**, 1291 (1972) [*Sov. Phys. JETP* **35**, 682 (1972)].
19. Y. R. Shen, *The Principles of Nonlinear Optics* (Wiley, New York, 1984; Nauka, Moscow, 1989).
20. G. Kh. Kitaeva, D. N. Klyshko, and I. V. Taubin, *Kvantovaya Élektron. (Moscow)* **9**, 560 (1982).
21. S. A. Akhmanov and R. V. Khokhlov, *Problems in Nonlinear Optics* (Akad. Nauk SSSR, Moscow, 1965; Gordon and Breach, New York, 1972).
22. M. Born and E. Wolf, *Principles of Optics*, 4th ed. (Pergamon Press, Oxford, 1969; Nauka, Moscow, 1970).
23. A. V. Burlakov, S. P. Kulik, A. N. Penin, and M. V. Chekhova, *Zh. Éksp. Teor. Fiz.* **113**, 1991 (1998) [*JETP* **86**, 1090 (1998)].
24. D. Yu. Korystov, S. P. Kulik, and A. N. Penin, *Kvantovaya Élektron. (Moscow)* **30**, 921 (2000).
25. A. V. Burlakov, Yu. B. Mamaeva, A. N. Penin, and M. V. Chekhova, *Zh. Éksp. Teor. Fiz.* **120**, 67 (2001) [*JETP* **93**, 55 (2001)].
26. D. Yu. Korystov, S. P. Kulik, and A. N. Penin, *Pis'ma Zh. Éksp. Teor. Fiz.* **73**, 248 (2001) [*JETP Lett.* **73**, 214 (2001)].
27. D. N. Klyshko, *Kvantovaya Élektron. (Moscow)* **4**, 1056 (1977).
28. D. N. Klyshko, *Kvantovaya Élektron. (Moscow)* **7**, 1932 (1980).
29. D. N. Klyshko and A. N. Penin, *Usp. Fiz. Nauk* **152**, 653 (1987) [*Sov. Phys.–Usp.* **30**, 716 (1987)].
30. O. A. Abroskina, G. Kh. Kitaeva, and A. N. Penin, *Dokl. Akad. Nauk SSSR* **280**, 584 (1985) [*Sov. Phys. Dokl.* **30**, 67 (1985)].
31. G. Kh. Kitaeva, A. V. Sergienko, and A. N. Penin, *Dokl. Akad. Nauk SSSR* **293**, 848 (1987) [*Sov. Phys. Dokl.* **32**, 293 (1987)].
32. R. Glauber, in *Quantum Optics and Electronics*, Ed. by C. DeWitt, A. Blandin, and C. Cohen-Tannoudji (Gordon and Breach, New York, 1965; Mir, Moscow, 1966).
33. *Surface Polaritons*, Ed. by V. M. Agranovich and D. L. Mills (North-Holland, Amsterdam, 1982; Nauka, Moscow, 1985).
34. V. N. Denisov, T. A. Leskova, B. N. Mavrin, and V. B. Podobedov, *Zh. Éksp. Teor. Fiz.* **94** (5), 261 (1988) [*Sov. Phys. JETP* **67**, 1013 (1988)].
35. Y. Sasaki and S. Ushioda, *Phys. Rev. B* **27**, 1122 (1983).
36. A. L. Aleksandrovskii, O. A. Gliko, I. I. Naumova, and V. I. Pryalkin, *Kvantovaya Élektron. (Moscow)* **23**, 657 (1996).
37. A. L. Aleksandrovskii, G. Kh. Kitaeva, S. P. Kulik, and A. N. Penin, *Zh. Éksp. Teor. Fiz.* **90**, 1051 (1986) [*Sov. Phys. JETP* **63**, 613 (1986)].
38. G. Kh. Kitaeva, S. P. Kulik, and A. N. Penin, *Fiz. Tverd. Tela (St. Petersburg)* **34**, 3440 (1992) [*Sov. Phys. Solid State* **34**, 1841 (1992)].
39. G. Kh. Kitaeva, S. P. Kulik, and A. N. Penin, *Ferroelectrics* **172**, 469 (1995).
40. G. Kh. Kitaeva, A. A. Mikhailovsky, I. I. Naumova, *et al.*, *Appl. Phys. B* **66**, 201 (1998).

Translated by A. Betev

SPELL: 1. sinc, 2. ?????????????????